Vol. 3, No. 3, pp. 267-283, (September 2022)
DOI: 10.21608/aujes.2022.145415.1076
Aswan University Journal of Environmental Studies (AUJES)
Online ISSN: 2735-4237, Print ISSN: 2735-4229
Journal homepage: https://aujes.journals.ekb.eg/ E-mail: AUJES@aswu.edu.eg
Original research

Synthesis of pure and palladium doped TiO_2 and their applications as modifiers for carbon paste electrode

Ahmed A. Abd El-Raady[1], Asmaa A. Khodari[2], Mohamed Nageeb Rashed[2]

[1]*Physical Chemistry Lab., Chemistry Department, Faculty of Science, South Valley University, Qena 83523, Egypt*
[2]*Chemistry Department, Faculty of Science, Aswan University, Aswan, Egypt*

Received: 18/6/2022 Accepted: 5/8/2022

Abstract:

TiO_2 was synthesized from titanium tetraisopropoxide in the presence of H_2O and H_2O_2 to form $TiO_{2(H2O)}$ and $TiO_{2(H2O2)}$ respectively. Thermo gravimetric analysis (TGA) was utilized to investigate the thermal stability and select proper calcination temperatures of the solid powders used to prepare the oxides. Accordingly, TiO_2 was obtained by calcination at 550 and 750°C. These oxides were characterized by TEM, XRD, FTIR, XRF and UV-Vis spectroscopy. Results showed that $TiO_{2(H2O2)}$ is more thermally stable than $TiO_{2(H2O)}$ and its nanoparticles are smaller. $TiO_{2(H2O2)(550)}$ was doped with palladium to form $Pd/TiO_{2(H2O2)(550)}$. The effect of palladium on the properties of $TiO_{2(H2O2)(550)}$ was discussed. Palladium showed no significant effect on the phase composition and crystal size of $TiO_{2(H2O2)550}$. However, the absorption onset wavelength of $Pd/TiO_{2(H2O2)550}$ was significantly red shifted compared to that of $TiO_{2(H2O٧)550}$. Pure and doped TiO_2 were used as modifiers for carbon paste electrode. Modification of carbon paste electrode with different pure and palladium doped TiO_2 resulted in a significant increase in the peak current and the electrochemical active surface area. Among all the modifiers used in this study, $Pd/TiO_{2(H2O2)550}$ showed the most significant effect on the electrode properties.

Keywords: TiO_2 nanoparticles, modified carbon paste electrode, Pd-doped TiO_2, nanoparticles, voltammetry.

1- Introduction

It is well known that chemical, physical, optical, electrical, and other properties of nanomaterial are significantly different from those of bulk materials due to their smaller sizes (1–100 nm). As a result of that nanomaterial have been widely used in different scientific and research fields. In analytical chemistry for instance, they are used for fabrication of new and better sensing devices (Tiwari *et al.*, 2009). Titanium dioxide, also known as titanium (IV) oxide or titania, is a mineral and a well-known semiconductor. In the nanosize, where one or more dimensions in the order of 100 nm in size or less (Zhao *et al.*, 2005) it exhibits excellent features.

Corresponding author*: E-mail address: smsmahmed11793@gamil.com

As a result of that and other features like easy manufacturing control, low cost, and non-hazardous nature, it has been extensively studied for applications in various fields. Solar cells, chemical sensors, pigments, self-cleaning surfaces, and environmental purification are among these fields (Bai *et al.*, 2014).

Titanium dioxide exists in the amorphous and crystalline forms. Anatase, rutile, and brookite are the most common crystalline polymorphs. The anatase and rutile phases are tetragonal, but the brookite phase is orthorhombic (Mahshid *et al.*, 2007). Rutile and anatase are the active crystallite phases of titanium dioxide (Liu *et al.*, 2009). Crystalline structures reveal certain physical properties which determine their applications and uses. Doping pure materials with proper quantities of some elements can significantly affect their crystalline structures and physical properties and hence the performance of these materials (Suo *et al.*, 2020).

Microemulsion, hydrothermal crystallization, and the sol–gel are examples of the suitable technologies utilized for the synthesis of TiO_2 of high surface area due to the formation of very low particle size (Gupta & Tripathi, 2012). The sol-gel method has been used to generate titanium dioxide nanoparticles and it is one of the most successful ways for the generation of nano-sized metals oxides. It was reported that the sol-gel prepared titanium dioxide nanoparticles are extremely crystalline and have smaller crystal sizes in comparison to those prepared by the previously mentioned technologies (Gupta & Tripathi, 2012). The nano sized TiO_2 used in this study was obtained from titanium tetraisopropoxide (TTIP) which is non-hazardous, non-toxic to the environment, stable and simple to use (Aravind *et al.*, 2021).

Carbon paste electrodes (CPEs) are widely employed in the field of electro analytical chemistry in recent years. They have many advantages like low cost, suitable surface properties, low background current, ease of surface renewal, proper polarizability, and ease of modification (Tiwari et al., 2009). Furthermore, using CPEs modified with many nanostructured components significantly improves the electrochemical behavior of many essential chemicals (Naeemy *et al.*, 2017; Nasikhudin *et al.*, 2017). In comparison, of nanoparticle modified electrodes with the conventional unmodified macroelectrodes, it becomes clear that the former has significant benefits such as larger effective surface area and mass transfer (Raj & Viswanathan, 2009). In this context using TiO_2 nanoparticles electrode modifiers attract considerable attention. Moreover, the incorporation of nano-sized substances like palladium (Pd) considerably improves the properties of such materials and it has been an active area of material preparation to develop material characteristics for applications like electrochemical sensor design (Chen, A. & Ostrom, 2015). In this study pure and palladium doped TiO_2 samples were synthesized, characterized and used as modifiers for carbon paste electrode.

2. Materials and Methods

2.1. Materials.

Titanium tetra isopropoxide ($Ti\{OCH(CH_3)_2\}_4$DAEJUNG, 98%), hydrogen peroxide (H_2O_2, Alpha chem., 50%), potassium chloride (KCl, 0.1 M), potassium hexacyanoferrate (III) ($K_3[Fe(CN)_6]$,1.0 mM), potassium hexacyanoferrate (II) ($K_4[Fe(CN)_6]$, 1.0 mM) were used in this study.

2.2. Apparatus.

A three- electrode system: the working electrode, the reference electrode (Ag/AgCl) and a Pt wire as a counter one with a computer-aided electrochemistry system were used in the

photometric studies. The computer-aided electrochemistry system consists of the following components:

1- A Versa STAT 4 (potentiostat/galvanostat) Princeton Applied Research.

2-A potentiostat model 263 (EG& G PARC) Princeton applied corporation (made in USA).
3-A 305 magnetic stirrer (PARC).
4- Electro analytical software model 270/250 version 4.0 (PARC) which controls the potentiostat via IEEE 488 GPIB using IBM compatible 386 with VGA monitor.

2.3. Characterization.

TGA was used to examine the thermal stability of the dried solid powders used for the synthesis of TiO_2 with a 30°C min^{-1} heating rate up to 800°C and a 100 mL min^{-1} Ar gas flow. The FTIR spectrum was obtained in the range 450 to 4000 cm^{-1} using Shimadzu FTIR, Kyoto, Japan. The phase structure and crystal sizes of TiO_2 NPs were determined using a powder x-ray diffractometer (X'Pert3 Powder, PAN alytical, The Netherlands) operating at 40 kV voltage and 30 mA current, monochromatic radiation (Cu-Kα, 1.5406 Å) with nickel monochromator, and a diffraction angle of 10-80°. The crystal sizes were calculated using the Scherrer′s equation ($D = K\lambda/\beta\cos\theta$). A Jeol Jem-1230 transmission electron microscope (TEM) was used to take images of TiO_2 NPs. Ultraviolet–Visible spectra were recorded with a UV 2300 double beam spectrophotometer in the range 200 and 800 nm. The existence of Pd in the synthesized TiO_2 sample was confirmed by the energy-dispersive X-ray fluorescence (ED-XRF, Epsilon 1; PANalytical).

2.4 Synthesis of TiO_2 samples:

2.4.1.Synthesis of $TiO_{2(H2O)}$:

$TiO_{2(H2O)}$ was synthesized from titanium tetra isopropoxide (TTIP) as follows: 5ml of TTIP was added to 10 ml of distilled water in a 500ml beaker and the mixture was stirred till a gel was formed. The gel was left to dry in air and then in an oven at 100 °C for 3 hrs. The dry solid formed was carefully milled and then was calcined at 550 and 750 °C. The resulting oxides were termed $TiO_{2(H2O)(550)}$ and $TiO_{2(H2O)(750)}$, respectively.

2.4.2.Synthesis of $TiO_{2\ (H2O2)}$:

$TiO_{2(H2O2)}$ was prepared from TTIP as follows: 5 ml of TTIP was added to 10 ml of H_2O_2 in a 500 ml beaker. The yellow precipitate formed was stirred for 2 hrs and left to dry in air and then in an oven at 100 °C for 3 hrs. The dry solid was milled and then calcined at 550 and 750 °C. The resulting oxides were termed $TiO_{2(H2O2)(550)}$ and $TiO_{2(H2O2)(750)}$, respectively.

2.4.3.Pd/$TiO_{2(H2O2)(550)}$

To prepare Pd/$TiO_{2(H2O2)(550)}$, the previous steps used for the preparation of $TiO_{2\ (H2O2)(500)}$ were repeated, but in addition, a calculated amount of palladium powder required to get 3.5 wt % of Pd in the final oxide sample was added to the dry yellow precipitate and the mixture was carefully mechanically mixed in a crucible and then calcined at 550°C for 3 hrs. to form Pd/$TiO_{2(H2O2)(550)}$

2.5 Preparation of the working electrodes.

i. Preparation of unmodified carbon paste electrode.

This electrode was prepared by mixing 75% of pure graphite (99.9%) with 25% paraffin wax as a binder. The mixture was heated, and the paste formed was packed in a Teflon tube with 3 mm diameter. Finally, a copper wire was immersed in the paste.

ii. Preparation of modified carbon paste electrodes:

The modified electrodes were prepared by mixing 60% of the pure graphite with 15% of different modifiers in the presence of 25% of the paraffin wax. The mixture was heated, and the paste formed was packed in a Teflon tube with ٣ mm diameter. Finally, a copper wire was immersed in the paste as seen in Fig.1. To activate the electrode surface, cyclic voltammograms were recorded in phosphate buffer solution (pH = 5) between 0 V and 1.0 V until a steady voltammogram was obtained.

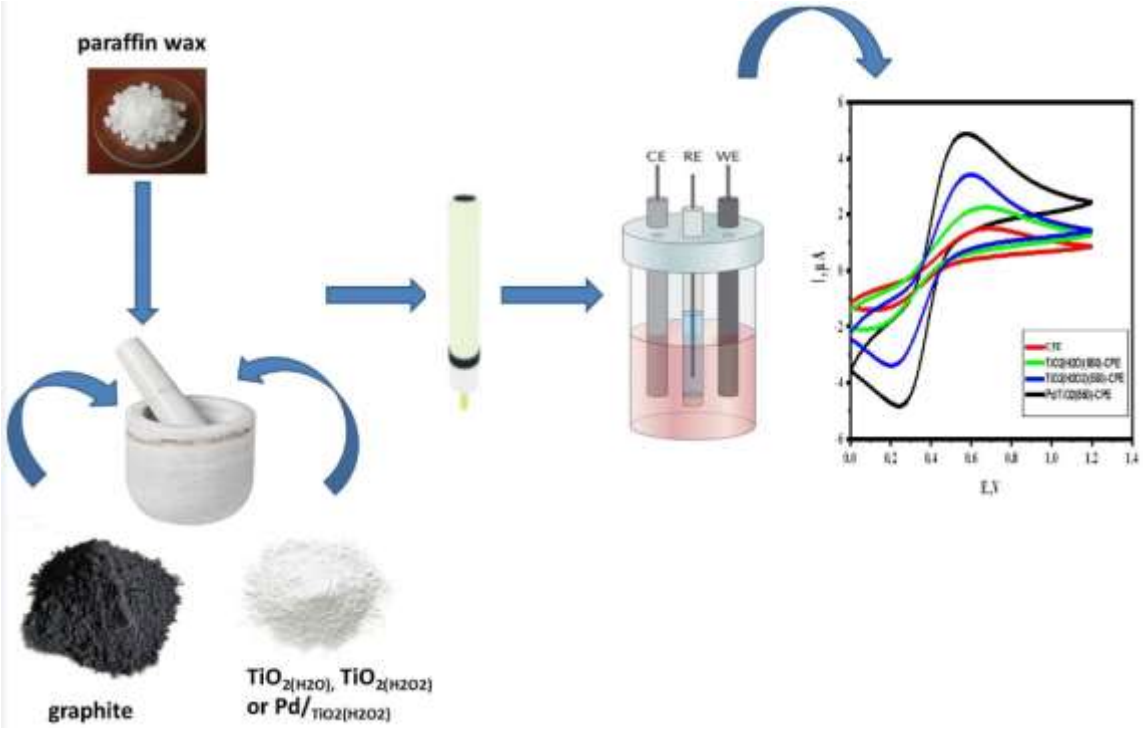

Figure 1. Schematic representation of the modified electrode and the electrochemical cell for CV experiments.

3. RESULTS AND DISCUSSION

3.1. Thermogravimetric Analysis

The TGA-DTG results of the solid powders used for the synthesis of $TiO_{2(H2O)}$ and $TiO_{2(H2O2)}$ are shown in Figure 2.a, b, respectively. Figure 2.a shows three distinct weight loss steps. These steps can be attributed, respectively, to the evaporation of physically adsorbed water, the combustion of organic molecules, and dehydroxylation (Zhu *et al.*, 2018). The DTG curve shows corresponding peaks as it is clear from Figure 2.a. Figure 2.b, on the other hand, shows a single steep weight loss step in the temperature range 100 - 400 ˚C. This step is accompanied

with about 23.5% weight loss. The corresponding DTG shows a single peak at 132˚C due to physical or chemical desorption of H_2O (dehydration) and the thermal decomposition of organic substrates (Dulian *et al.*, 2020). These results indicate that calcination at around 500°C is suitable for the creation of the oxides.

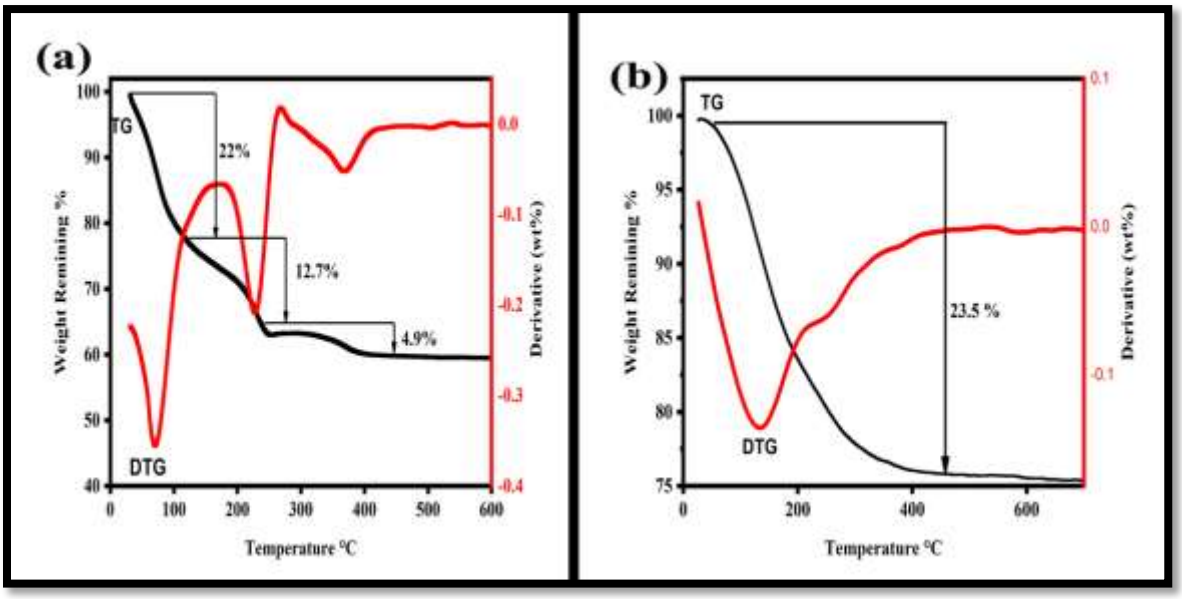

Figure 2. TGA, DTG curves of the solid powder used for the preparation of (a) $TiO_{2(H2O)}$ and (b) $TiO_{2(H2O2)}$.

3.2. X-ray diffraction analysis

Fig.3. presents the XRD patterns of different TiO_2 samples. Table (1) shows the phase composition and mean crystallite size of different samples estimated from XRD data using the Debye Scherrer's equation (Chen, X. & Mao, 2007). It is obvious from these patterns that $TiO_{2(H2O)\ (550)}$ consists of anatase phase as a single phase. $TiO_{2(H2O)\ (750)}$, on the other hand, contains a mixture of anatase and rutile. This effect of increasing calcinations temperature on the phase composition is known (Velardi *et al.*, 2020; Wu *et al.*, 2020). It is also clear that as the calcination temperature increases from 550°C to 750°C, the peaks intensities increase, and the peaks widths narrow due to increasing particle sizes at the higher temperatures. Table (1) shows that when the calcination temperature was increased from 550 °C to 750 ˚C the average crystallite size of the oxides increased from 24.27 nm to 73.69 nm.

Many routs for the synthesis of thermally stable anatase phase were reported in the literature (Nagaraj *et al.*, 2020; Wei *et al.*, 2013). A thermally stable anatase phase was obtained in case of $TiO_{2(H2O2)}$. Figure (3) shows the XRD patterns of $TiO_{2(H2O2)}$ samples calcined at 550 and 750°C. The two samples contain anatase as a single phase. This result indicates that the anatase phase produced by this method has a higher thermal stability. The mean crystal size of $TiO_{2(H2O2)550}$ and $TiO_{2(H2O2)750}$, calculated from the XRD data using the Sherrer's equation, are also shown in Table 1. The mean crystal sizes were calculated to be 12.4 and 25.6 nm, respectively.

Palladium doping of TiO_2 was reported (Lakshminarayana *et al.*, 2018; Li *et al.*, 2016; Tu *et al.*, 2019; Xiong *et al.*, 2022). Doping was reported to affect peak properties like peak

broadening (Singh *et al.*, 2019). Others reported that there is no large effect of doping on the peak characteristics (Abd El-Rady *et al.*, 2013; Zhong *et al.*, 2009). The XRD pattern of $Pd/TiO_{2(H2O2)(550)}$ is also presented in Figure 3. There is no significant effect of palladium on the phase composition or peak intensities. Also. No peaks due to palladium were observed in the XRD pattern. This may be due to that palladium content is small and it is homogenously dispersed in the sample.

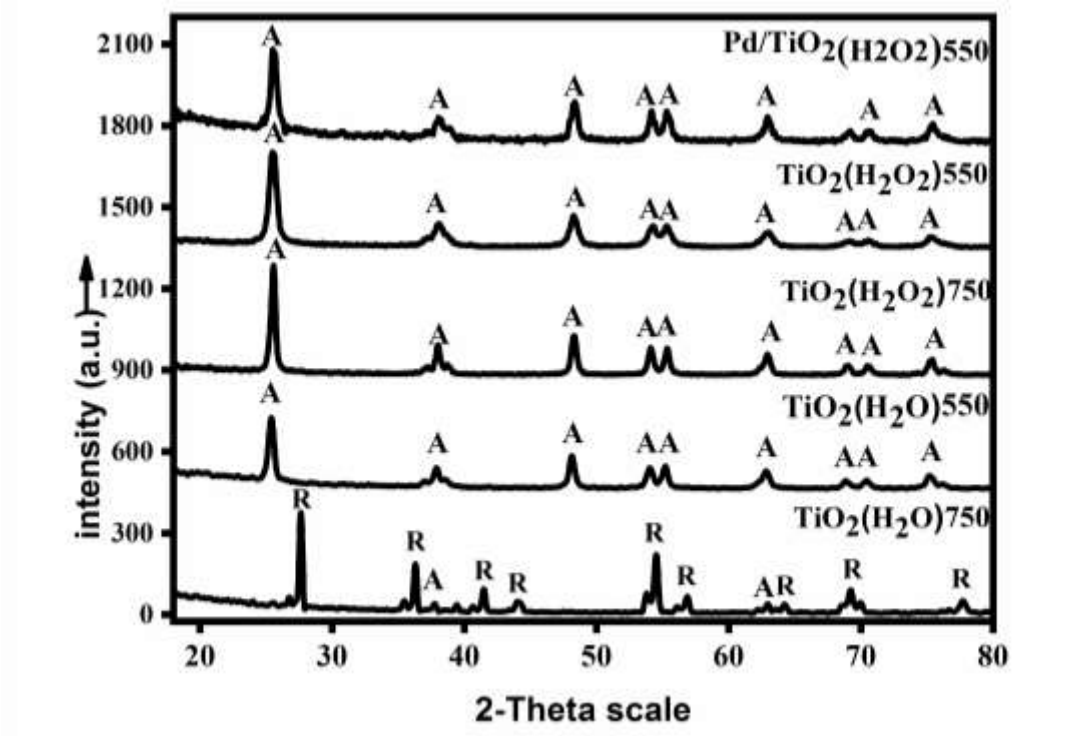

Figure 3. XRD pattern of different TiO_2 samples

Table 1: XRD data for different TiO_2 samples

Sample	Crystalline phase	Crystal shape	Crystal size nm
$TiO_{2(H2O)(550)}$	anatase	Hexagonal	24.27
$TiO_{2(H2O)(750)}$	anatase, rutile	Hexagonal	73.69
$TiO_{2(H2O2)(550)}$	anatase	Hexagonal	12.38
$TiO_{2(H2O2)(750)}$	anatase	Hexagonal	25.66
$Pd/_{TiO2(H2O2)(550)}$	anatase	Hexagonal	15.9

3.3. Fourier Transform Infrared Spectroscopy (FTIR).

The FTIR spectra of different TiO_2 samples are shown in Fig.4. These spectra show broad peaks at 3320-3425 cm^{-1} due to OH stretching mode (Chougala *et al.*, 2017; Praveen *et al.*, 2014). The bands at 1615-1635 cm^{-1} correspond to the O-H bending vibration of the group due to chemically adsorbed water (Zewde *et al.*, 2016). The broad peaks at 480-560 cm^{-1} are due to the Ti-O band. It was reported that when TiO_2 was doped with metal ions, a small shift was observed for the stretching vibration band of Ti–O (Nasikhudin et al., 2017,Singh et al., 2019). It is noticeable that the Ti-O band of $Pd/TiO_{2(H2O2)(550)}$ in figure 4 is slightly shifted

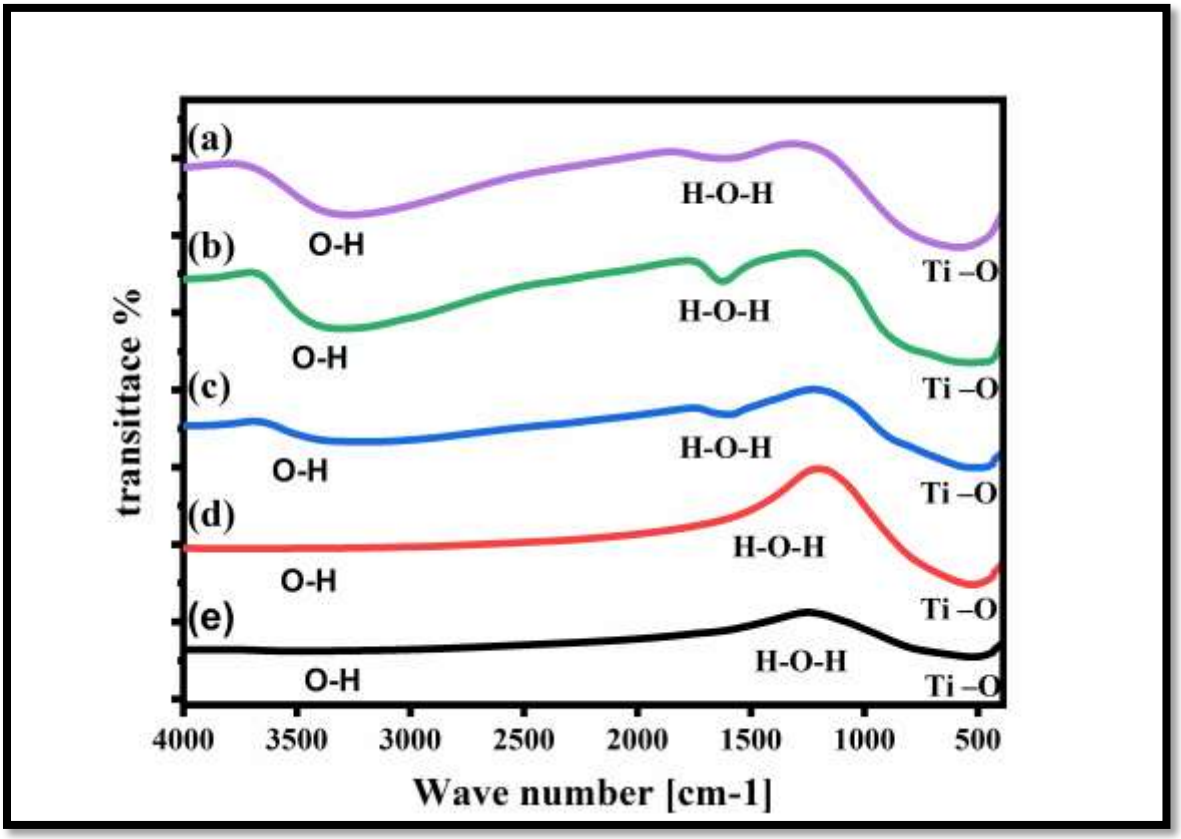

Figure 4. FT-IR spectra of different samples (a) $Pd/TiO_{2(H2O2)\,(550)}$, (b) $TiO_{2(H2O2)(550)}$, (c) $TiO_{2\,(H2O2)(750)}$, (d) $TiO_{2\,(H2O)\,(550)}$ and (e) $TiO_{2\,(H2O)\,(750)}$

3.4. Transmission Electron Microscopy (TEM).

Fig.5. shows the TEM images of different TiO_2 samples. As can be seen from this figure, the particles in all samples are spherical and uniform in shape. It's also clear that the particle sizes are in the nanoscale, which agrees with the results of crystall sizes calculated from the XRD data.

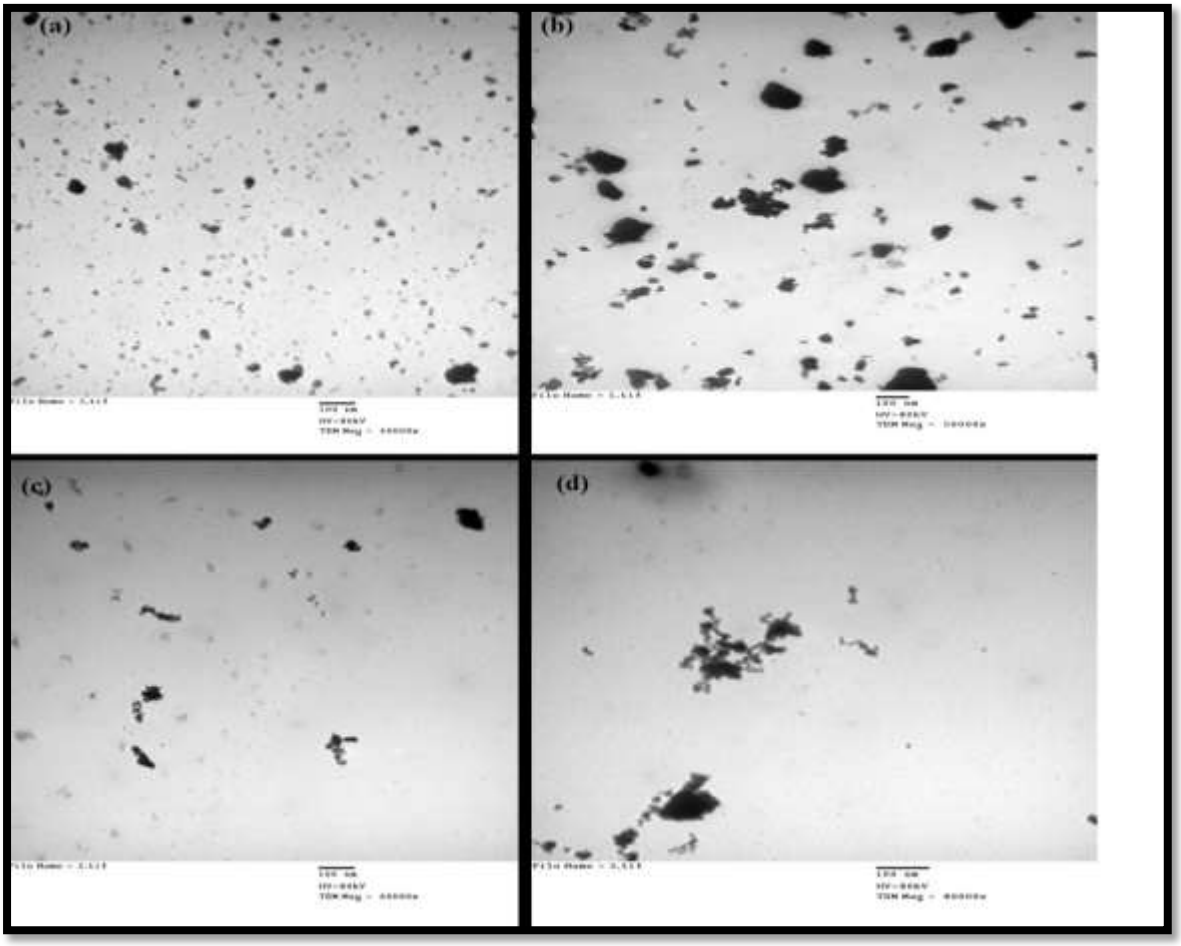

Figure 5. TEM images of (a)$TiO_{2\ (H2O)\ (550)}$,(b) $TiO_{2\ (H2O)(750)}$, (c)$TiO_{2\ (H2O2)(550)}$ and $TiO_{2\ (H2O2)(750)}$

3.5 UV–Vis spectroscopy.

Fig.6. Shows the UV-visible absorption spectra of different TiO_2 samples. Extrapolation of the base line and the absorption edge of these spectra yields the absorption onset wavelength (λ). As the calcination temperature increased, the onset wavelength of absorptions was shifted to longer wavelengths (red shifted) and a corresponding decrease in the band gap energy was observed (Mioduska *et al.*, 2016; Reyes-Coronado *et al.*, 2008). Furthermore, it is noticeable that when compared to the pure TiO_2, the inclusion of palladium has a considerable impact on the spectrum as presented in Figure 6 (d and f). Figure 7 illustrates Tauc′s plots for the different tested samples and Table 2 displays the onset wavelength of absorption as well as the values of band gaps energies of different samples.

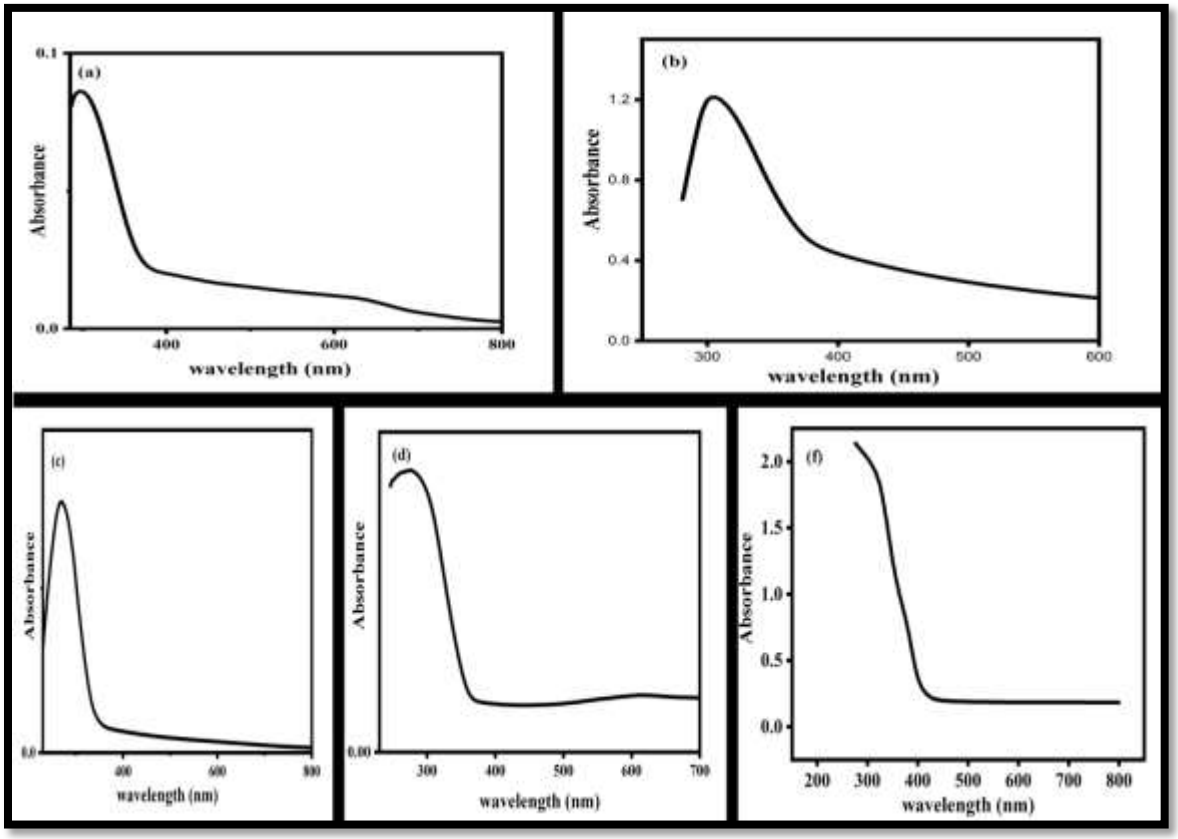

Figure 6. UV-Vis absorption spectrum of (a) $TiO_{2(H2O)\,(550)}$, (b) $TiO_{2(H20)(750)}$, (c) $TiO_{2(H2O2)(550)}$ and (d) $TiO_{2(H2O2)(750)}$ and (f) $Pd/TiO_{2(H2O2)(550)}$

Table 2: The onset wavelength of absorption and the corresponding band gap energies of different TiO_2 samples.

Sample	Onset wavelength of absorption(nm)	theoretical band gap (eV)	experimental band gap (eV)
$TiO_{2\,(H2O)\,(550)}$	**376**	**3.3**	**3.34**
$TiO_{2\,(H20)\,(750)}$	**386**	**3.21**	**3.25**
$TiO_{2\,(H2O2)\,(550)}$	**364**	**3.41**	**3.4**
$TiO_{2\,(H2O2)\,(750)}$	**370**	**3.35**	**3.34**
$Pd/TiO_{2\,(H2O2)\,(550)}$	**385**	**3.22**	**3.26**

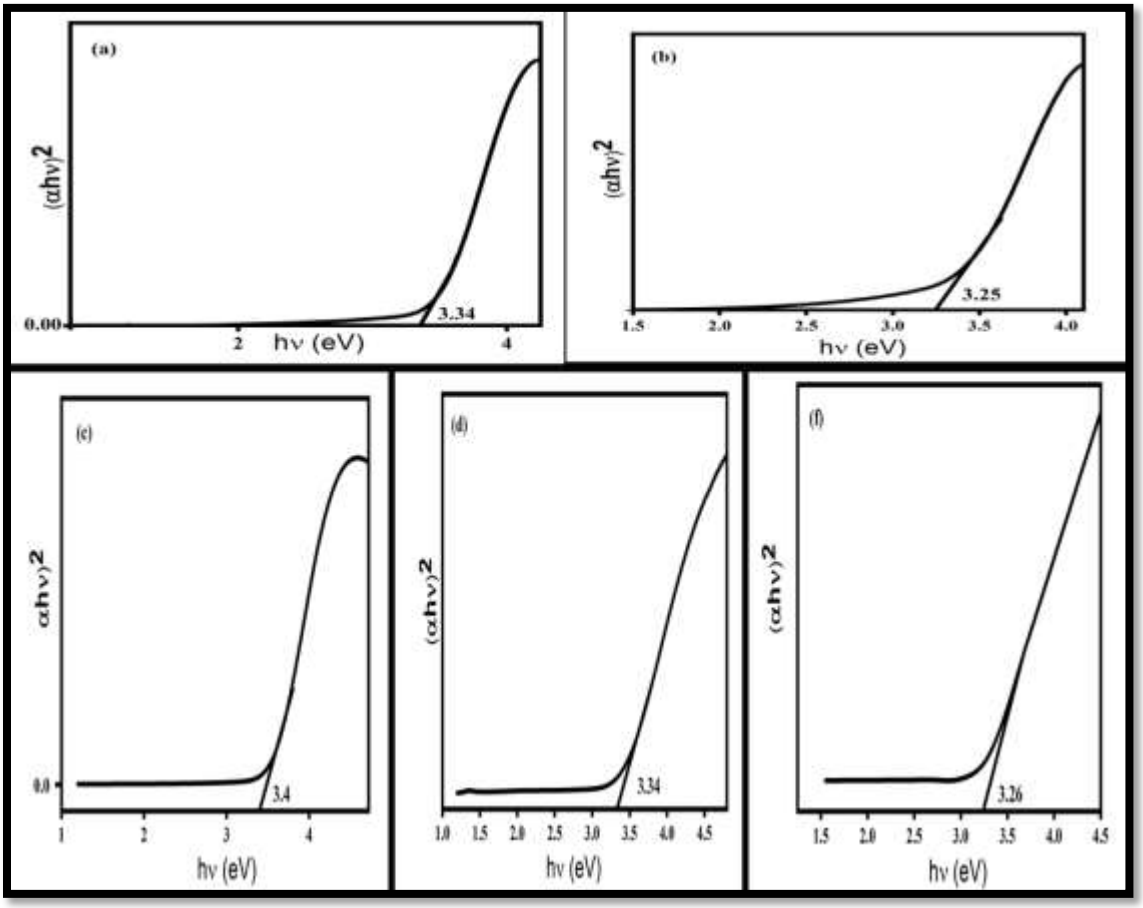

Figure 7. plot of $(\alpha h\nu)^2$ versus photon energy (hν) of (a) $TiO_{2(H2O)\,(550)}$, (b) $TiO_{2(H20)(750)}$, (c) $TiO_{2\,(H2O2)(550)}$ and (d) $TiO_{2\,(H2O2)(750)}$ and $Pd/TiO_{2\,(H2O2)(550)}$.

3.6 X-ray fluorescence spectroscopy.

XRF analysis was used to confirm the existence of Pd in the synthesized $Pd/TiO_{2(H2O2)\,(550)}$ sample, and the result is shown in Figure 8. Similar result was observed by others (Soman *et al.*, 2018).

3.7. Voltammetric performance of the electrodes.

The electron transfer behavior of the modified electrodes can be explained and monitored using the CV of potassium hexacyanoferrate. The electron transport tunnelling via imperfections on the electrode surface may be facilitated by modification or pretreatment of the electrode (Fu *et al.*, 2005). In this study, the electrodes were voltammetrically evaluated in the presence of 0.1 M KCl and 1 mM $[Fe\,(CN)_6]^{3-/4-}$ as an electrochemical probe. CVs of unmodified and modified CPEs ($TiO_{2(H2O)\,(550)}$-CPE , $TiO_{2(H2O2)(550)}$-CPE and $Pd/TiO_{2(H2O2)(550)}$-CPE) at a scan rate of 50 $mV.s^{-1}$ are shown in Figure 9. Modified CPEs showed superior electroactive performance compared to the unmodified CPE. As can be seen from the figure, these sensors show a significant increase in the faradaic anodic and cathodic peaks currents. Moreover, the peak potential variation (ΔE_p) can be associated with the electron transfer kinetics between the electrochemical probe and the electrode surface. The values of redox peak currents and potentials are summarized in table 3. As can be seen, these electrodes exhibited a decrease in ΔE_p values.

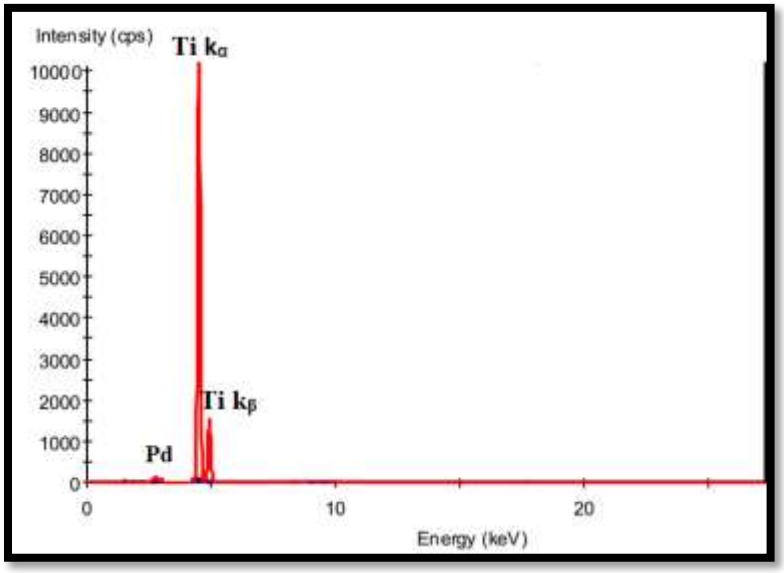

Figure 8. XRF spectrum of $Pd/TiO_{2(H2O2)(550)}$.

Table 3: The values of redox peak currents and potentials

Electrode	Current (µA)		Potential (V)		ΔE_p
	I_p ox	I_p red	P_{ox}	P_{red}	
CPE	1.5	-1.4	0.7	0.1	0.6
$TiO_{2(H2O)\ (550)}$ – CPE	2.25	-2.1	0.66	0.09	0.55
$TiO_{2(H2O2)\ (550)}$ – CPE	3.41	-3.38	0.59	0.2	0.39
$Pd/TiO_{2(H2O2)\ (550)}$	5.9	-5.5	0.57	0.4	0.17

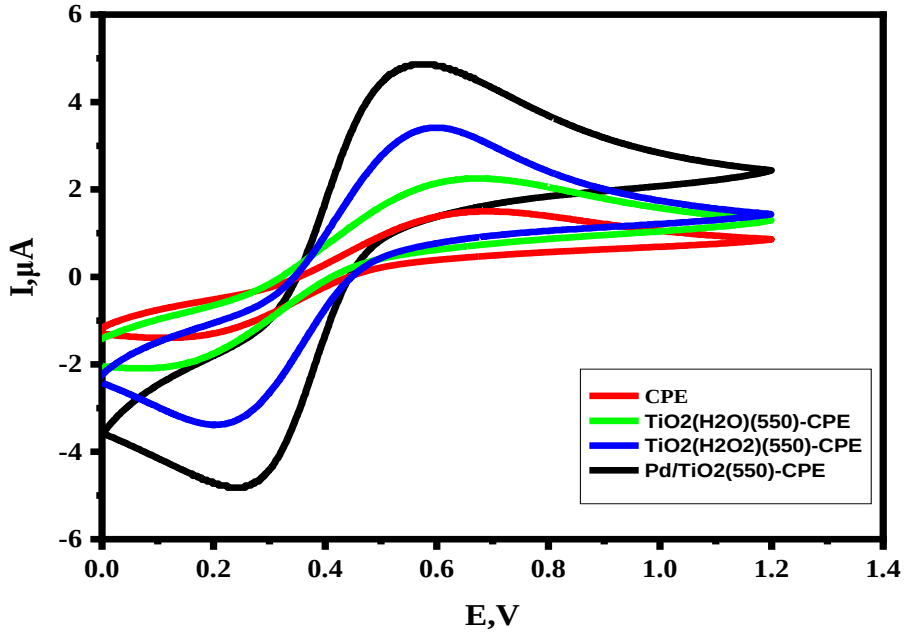

Figure 9. CVs of 5×10^{-3} M $K_3[Fe(CN)_6]$ in 0.1 M KCl at unmodified CPE, $TiO_{2(H2O)(550)}$ – CPE, $TiO_{2(H2O2)(550)}$ – CPE and $Pd/TiO_{2(H2O2)(550)}$ – CPE

3.7.1 Determination of electroactive surface areas

To determine the electroactive surface area of the unmodified CPE, $TiO_{2(H2O)\ (550)}$-CPE , $TiO_{2(H2O2)(550)}$-CPE and pd/$TiO_{2(550)(550)}$-CPE electrodes, CVs of 1×10^{-3} M $K_3[Fe\ (CN)_6]$ in 0.1 M KCl were recorded at various scan rates. Then, Randles-Sevcik formula was used for surface area estimation (Naeemy et al., 2017).

$$\mathbf{Ip_a = (2.69 \times 10^5)\ n^{3/2}\ ACD^{1/2}v^{1/2}}$$

In the previous equation, Ip_a is the current response for 1×10^{-3} M $K_3[Fe(CN)_6]$, n is the number of electrons involved in the redox process of $K_3[Fe(CN)_6]$, A is the electrode surface area, C is the analytical concentration of $K_3[Fe(CN)_6]$ in 0.1 M KCl, D is the diffusion coefficient (= 7.6×10^{-6} $cm^2\ s^{-1}$), and *v* is the scan rate (mV. s^{-1}).

Figure 10 shows CVs of $K_3[Fe\ (CN)_6]$ at various scan rates for unmodified CPE (**A**). The slope of I_p vs. $v^{1/2}$ was utilized for calculation of the electro active surface area for the electrode (**Figure 10.B). Figures (11-13)** show CVs of $K_3[Fe\ (CN)_6]$ at various scan rates for $TiO_{2(H2O)\ (550)}$ -CPE, $TiO_{2(H2O2)\ (550)}$-CPE and $Pd/TiO_{2(H2O2)\ (550)}$-CPE, respectively. The experimental results gave electro active surface areas of 0.088, 0.147, 0.29 and 0.46 cm^2, for CPE, $TiO_{2(H2O)\ (550)}$-CPE, $TiO_{2(H2O2)\ (550)}$-CPE and pd/$TiO_{2(550)}$-CPE electrodes, respectively. Obviously, the peak current and the electrochemically active surface area of the unmodified electrode is greatly increased as a result of modification especially in the case of $pd/TiO_{2(H2O2)\ (550)}$-CPE. Thus, these modified electrodes probably can be employed efficiently for the electrochemical sensing of a wide variety of analytes in different matrices.

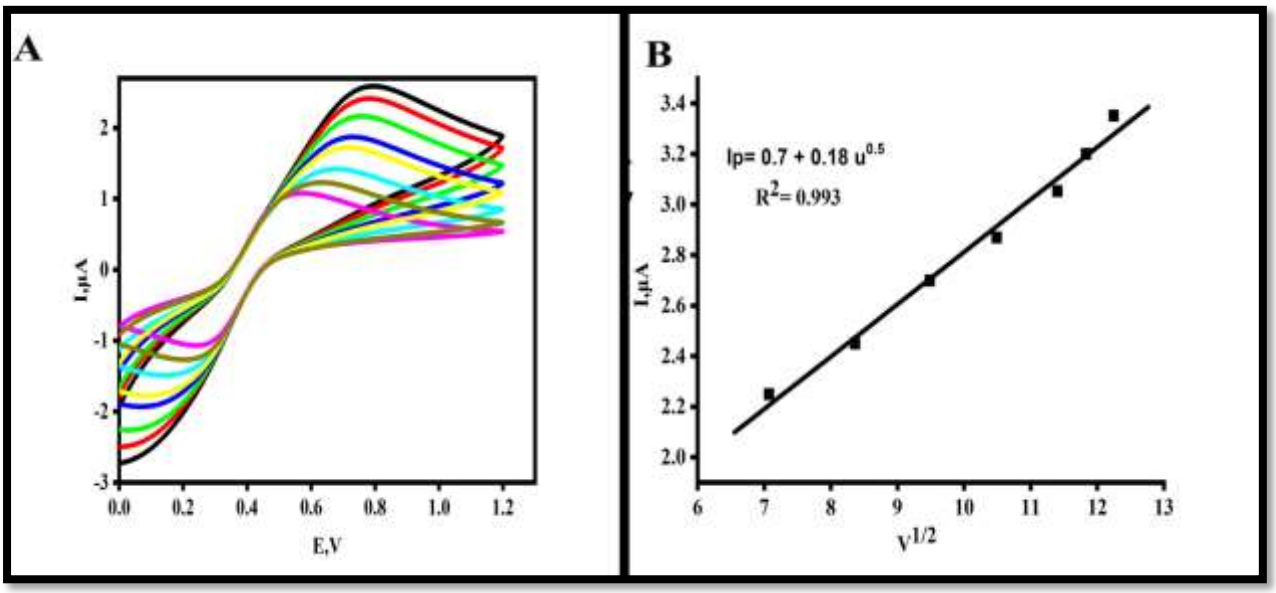

Figure 10. CVs of 5×10^{-3} M $K_3[Fe\ (CN)6]$ in 0.1 M KCl at (A) unmodified CPE at scan rates of 10, 20, 30, 40, 50, 75, and 100 mVs^{-1}. A plot of peak current versus square root of scan rate of (B)

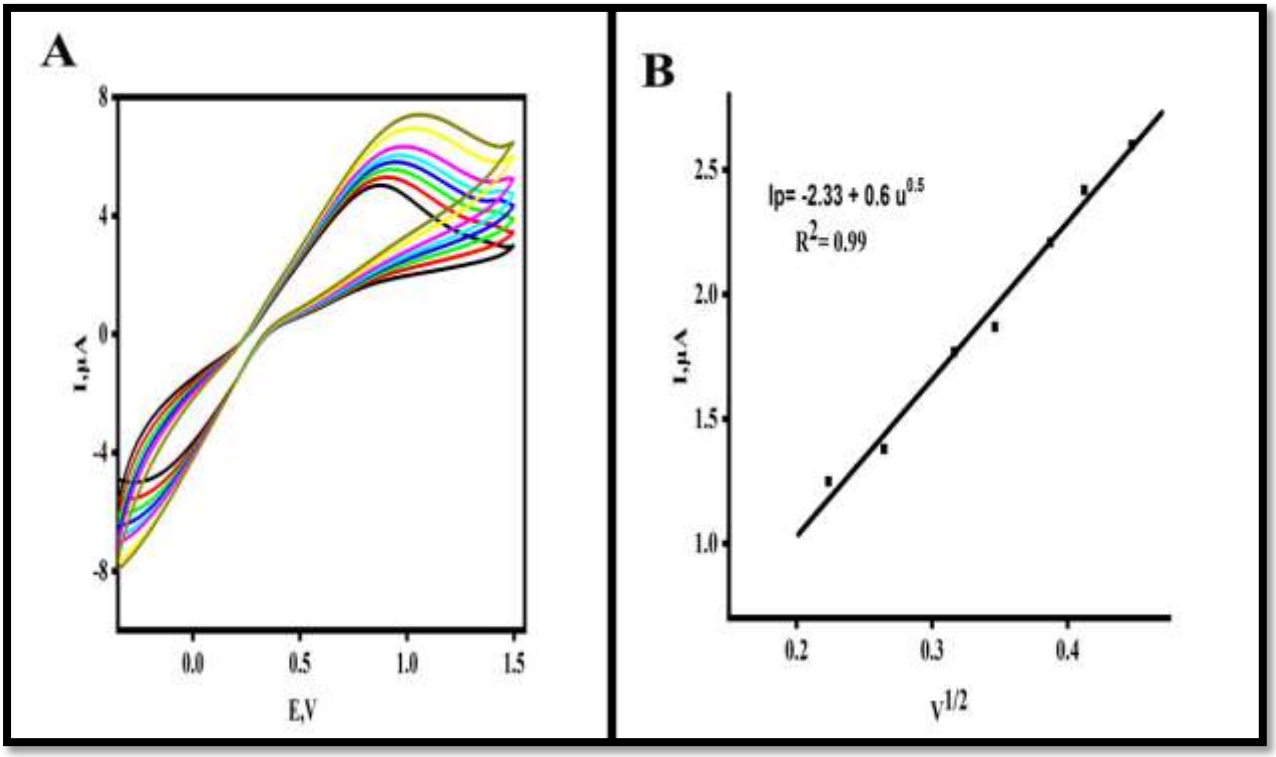

Figure 11. CVs of 5×10^{-3} M K_3[Fe (CN)6] in 0.1 M KCl at (A) $TiO_{2(H2O)\,(550)}$-CPE at scan rates of 10, 20, 30, 40, 50, 75, and 100 mV/s. A plot of peak current versus square root of scan rate of (B).

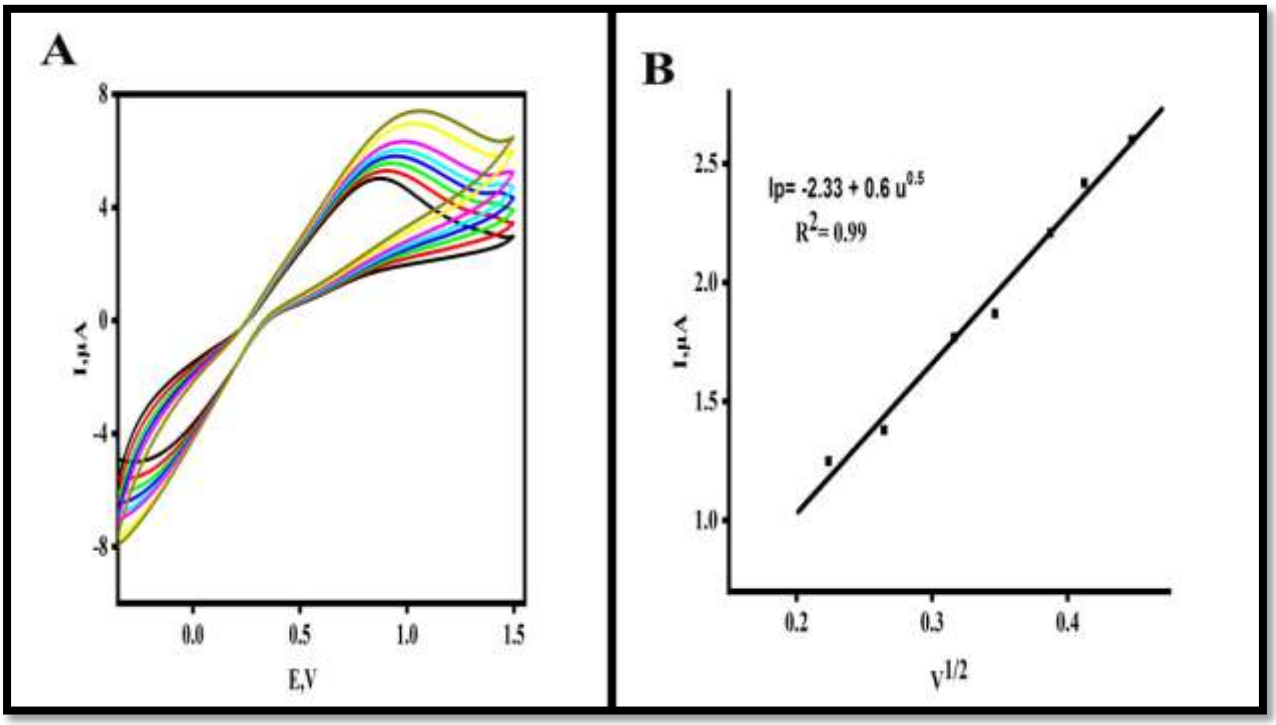

Figure 12. CVs of 5×10^{-3} M $K_3[Fe(CN)_6]$ in 0.1 M KCl at (A) $TiO_{2(H2O2)\,(550)}$-CPE at scan rates of 10, 20, 30, 40, 50, 75, and 100 mVs^{-1}. A plot of peak current versus square root of scan rate of (B).

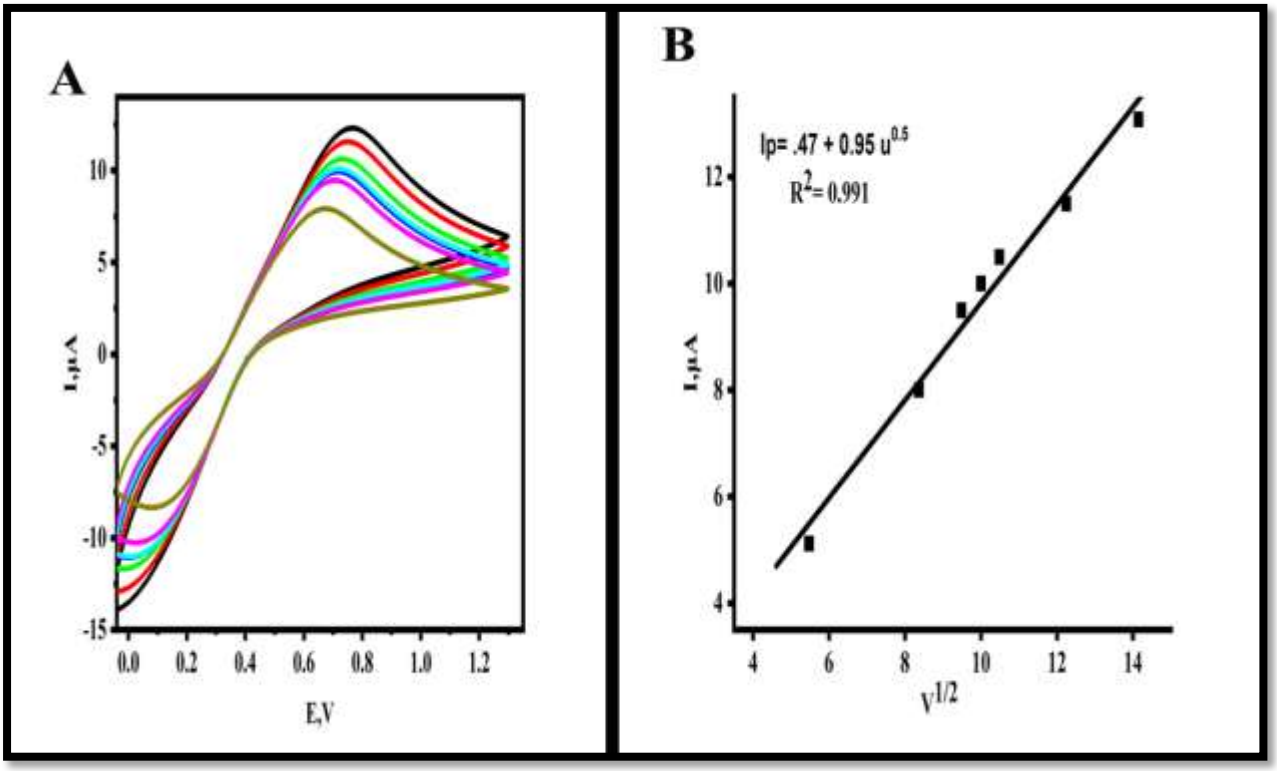

Figure 13. CVs of 5×10^{-3} M K_3[Fe (CN)6] in 0.1 M KCl at (A) Pd/$TiO_{2(550)}$-CPE at scan rates of 10, 20, 30, 40, 50, 75, and 100 mVs^{-1}. A plot of peak current versus square root of scan rate of (B).

4. Conclusion

In this study pure titanium oxides ($TiO_{2(H2O2)}$ and $TiO_{2(H2O)}$) were synthesized and characterized. The effect of calcination temperature (550 and 750°C) on the characteristics of these oxides was discussed. The anatase phase of $TiO_{2(H2O2)}$ is more stable than that of $TiO_{2(H2O)}$ and the samples calcined at the lower temperature (550°C) showed superior properties than those calcined at the higher temperature (750°C). Therefore, $TiO_{2(H2O2)(550)}$ was chosen for doping with palladium. The effect of palladium inclusion on the properties of TiO_2 was discussed. The effects of pure and Pd doped TiO_2 on the characteristics of CBE were evaluated.

Modification of the carbon paste electrode with $TiO_{2(H2O)550,}$ $TiO_{2(H2O2)\ (550)}$ and $Pd/TiO_{2(H2O2)550}$ resulted in a significant increase in the peak current and the electrochemically active surface area. The relative efficiency of these modifiers to enhance peak current and electro active surface area follows the following order: $TiO_{2(H2O)(550)}$< $TiO_{2(H2O2)\ (550)}$ < $Pd/TiO_{2(H2O2)(550)}$.

References

Abd El-Rady, A.A., Abd El-Sadek, M.S., El-Sayed Breky, M.M.and Assaf, F.H. 2013. "Characterization and Photocatalytic Efficiency of Palladium Doped-$TiO_2$₂ Nanoparticles" *Advances in Nanoparticles, 02*04, 372-377. doi:10.4236/anp.2013.24051.

Aravind, M., Amalanathan, M.andMary, M.S.M. 2021. "Synthesis of TiO_2 nanoparticles by chemical and green synthesis methods and their multifaceted properties" *SN Applied Sciences, 3*4. doi:ARTN 40910.1007/s42452-021-04281-5.

Bai, Y., Mora-Sero, I., De Angelis, F., Bisquert, J.andWang, P. 2014. "Titanium dioxide nanomaterials for photovoltaic applications" *Chem Rev, 114*19, 10095-10130. doi:10.1021/cr400606n.

Chen, A.andOstrom, C. 2015. "Palladium-Based Nanomaterials: Synthesis and Electrochemical Applications" *Chem Rev, 115*21, 11999-12044. doi:10.1021/acs.chemrev.5b00324.

Chen, X.andMao, S.S. 2007. "Titanium dioxide nanomaterials: synthesis, properties, modifications, and applications" *Chem Rev, 107*7, 2891-2959. doi:10.1021/cr0500535.

Chougala, L.S., Yatnatti, M.S., Linganagoudar, R.K., Kamble, R.R.andKadadevarmath, J.S. 2017. "A Simple Approach on Synthesis of TiO2 Nanoparticles and its Application in dye Sensitized Solar Cells" *Journal of Nano- and Electronic Physics, 9*4. doi:ARTN 0400510.21272/jnep.9(4).04005.

Dulian, P., Zajic, J.andŻukowski, W. 2020. "Effect of titanium source and sol-gel TiO2 thin film formation parameters on its morphology and photocatalytic activity" *Materials Science-Poland, 38*3, 424-433. doi:10.2478/msp-2020-0056.

Fu, Y., Yuan, R., Tang, D., Chai, Y.andXu, L. 2005. "Study on the immobilization of anti-IgG on Au-colloid modified gold electrode via potentiometric immunosensor, cyclic voltammetry, and electrochemical impedance techniques" *Colloids Surf B Biointerfaces, 40*1, 61-66. doi:10.1016/j.colsurfb.2004.10.022

Gupta, S.andTripathi, M. 2012. "A review on the synthesis of TiO2 nanoparticles by solution route" *Open Chemistry, 10*2, 279-294. doi:10.2478/s11532-011-0155-y

Lakshminarayana, B., Satyanarayana, G.andSubrahmanyam, C. 2018. "Bimetallic Pd-Au/TiO2 Nanoparticles: An Efficient and Sustainable Heterogeneous Catalyst for Rapid Catalytic Hydrogen Transfer Reduction of Nitroarenes" *ACS Omega, 3*10, 13065-13072. doi:10.1021/acsomega.8b02064

Li, C., Zong, L., Li, Q., Zhang, J., Yang, J.andJin, Z. 2016. "Photocatalytic Oxidation of Propylene on Pd-Loaded Anatase TiO2 Nanotubes Under Visible Light Irradiation" *Nanoscale Res Lett, 11*1, 271. doi:10.1186/s11671-016-1486-6

Liu, G., Wang, X., Chen, Z., Cheng, H.M.andLu, G.Q. 2009. "The role of crystal phase in determining photocatalytic activity of nitrogen doped TiO2" *J Colloid Interface Sci, 329*2, 331-338. doi:10.1016/j.jcis.2008.09.061

Mahshid, S., Askari, M.andGhamsari, M.S. 2007. "Synthesis of TiO2 nanoparticles by hydrolysis and peptization of titanium isopropoxide solution" *Journal of Materials Processing Technology, 189*1-3, 296-300. doi:10.1016/j.jmatprotec.2007.01.040

Mioduska, J., Zielińska-Jurek, A., Janczarek, M.andHupka, J. 2016. "The Effect of Calcination Temperature on Structure and Photocatalytic Properties of WO3/TiO2Nanocomposites" *Journal of Nanomaterials, 2016*, 1-8. doi:10.1155/2016/3145912

Naeemy, A., Mohammadi, A.andAssi, N. 2017. "Voltammetric determination of paracetamol at NiO nanoparticles-modified carbon paste electrode in bulk and tablet dosage forms" *Journal of Analytical Chemistry, 727*, 783-792. doi:10.1134/s1061934817070024

Nagaraj, G., Brundha, D., Chandraleka, C., Arulpriya, M., Kowsalya, V., Sangavi, S., Jayalakshmi, R., Tamilarasu, S.andMurugan, R. 2020. "Facile synthesis of improved

anatase TiO2 nanoparticles for enhanced solar-light driven photocatalyst" *SN Applied Sciences, 2*4. doi:10.1007/s42452-020-2554-1

Nasikhudin, Ismaya, E.P., Diantoro, M., Kusumaatmaja, A.andTriyana, K. 2017. "Preparation of PVA/TiO2 Composites Nanofibers by using Electrospinning Method for Photocatalytic Degradation" *4th International Conference on Advanced Materials Science and Technology, 2016, 202*. doi:Artn 01201110.1088/1757-899x/202/1/012011

Penn, S.G., He, L.andNatan, M.J. 2003. "Nanoparticles for bioanalysis" *Curr Opin Chem Biol, 7*5, 609-615. doi:10.1016/j.cbpa.2003.08.013

Praveen, P., Viruthagiri, G., Mugundan, S.andShanmugam, N. 2014. "Structural, optical and morphological analyses of pristine titanium di-oxide nanoparticles--synthesized via sol-gel route" *Spectrochim Acta A Mol Biomol Spectrosc, 117*, 622-629. doi:10.1016/j.saa.2013.09.037

Raj, K.J.A.andViswanathan, B. 2009. "Effect of surface area, pore volume and particle size of P25 titania on the phase transformation of anatase to rutile" *Indian Journal of Chemistry Section a-Inorganic Bio-Inorganic Physical Theoretical & Analytical Chemistry, 48*10, 1378-1382. doi:10.1002/elan.200302930

Reyes-Coronado, D., Rodriguez-Gattorno, G., Espinosa-Pesqueira, M.E., Cab, C., de Coss, R.andOskam, G. 2008. "Phase-pure TiO(2) nanoparticles: anatase, brookite and rutile" *Nanotechnology, 19*14, 145605. doi:10.1088/0957-4484/19/14/145605

Singh, B., Arya, S., Sharma, A., Mahajan, P., Gupta, J., Singh, A., Verma, S., Bandhoria, P.andBharti, V. 2019. "Effect of Pd concentration on the structural, morphological and photodiode properties of TiO2 nanoparticles" *Journal of Materials Science: Materials in Electronics, 31*1, 65-74. doi:10.1007/s10854-019-01095-5

Soman, B., Challagulla, S., Payra, S., Dinda, S.andRoy, S. 2018. "Surface morphology and active sites of TiO2 for photoassisted catalysis" *Research on Chemical Intermediates, 44*4, 2261-2273. doi:10.1007/s11164-017-3227-6

Suo, Z., Dai, J., Gao, S.andGao, H. 2020. "Effect of transition metals (Sc, Ti, V, Cr and Mn) doping on electronic structure and optical properties of CdS" *Results in Physics, 17*. doi:10.1016/j.rinp.2020.103058

Tiwari, I., Singh, K.P.andSingh, M. 2009. "An insight review on the application of polymer-carbon nanotubes based composite material in sensor technology" *Russian Journal of General Chemistry, 79*12, 2685-2694. doi:10.1134/S1070363209120226

Tu, L.N.Q., Nhan, N.V.H., Van Dung, N., An, N.T.andLong, N.Q. 2019. "Enhanced photocatalytic performance and moisture tolerance of nano-sized Me/TiO2–zeolite Y (Me=Au, Pd) for gaseous toluene removal: activity and mechanistic investigation" *Journal of Nanoparticle Research, 21*9. doi:10.1007/s11051-019-4642-y

Velardi, L., Scrimieri, L., Serra, A., Manno, D.andCalcagnile, L. 2020. "Effect of temperature on the physical, optical and photocatalytic properties of TiO2 nanoparticles" *SN Applied Sciences, 2*4. doi:ARTN 70710.1007/s42452-020-2544-3

Wei, X., Zhu, G., Fang, J.andChen, J. 2013. "Synthesis, Characterization, and Photocatalysis of Well-Dispersible Phase-Pure Anatase TiO2Nanoparticles" *International Journal of Photoenergy, 2013*, 1-6. doi:10.1155/2013/726872

Wu, Y.T., Liu, T.T., Yuan, J., Liu, C.Q., Wu, P.H., Lu, J.andWang, X.F. 2020. "The preparation and study of multilayer structured SiO2-TiO2 film: the effects of photonic crystals on enhanced photocatalytic properties" *Journal of Materials Science, 55*25, 11095-11105. doi:10.1007/s10853-020-04836-8

Xiong, R., Cheng, M., Wang, R., Tao, L., Wang, Z.andZhang, M. 2022. "A Carbon Shell Covered Pd Catalyst for Hydrogenation of 4-Nitrothioanisole" *Catalysis Letters*. doi:10.1007/s10562022-03925-4

Zewde, B., Pitliya, P.andRaghavan, D. 2016. "The role of surface modified TiO2 nanoparticles on the mechanical and thermal properties of CTBN toughened epoxy nanocomposite" *Journal of Materials Science, 51*20, 9314-9329. doi:10.1007/s10853-016-0179-y

Zhao, J., Wang, X., Sun, T.andLi, L. 2005. "In situ templated synthesis of anatase single-crystal nanotube arrays" *Nanotechnology, 16*10, 2450-2454. doi:10.1088/09574484/16/10/077

Zhong, J.B., Lu, Y., Jiang, W.D., Meng, Q.M., He, X.Y., Li, J.Z.andChen, Y.Q. 2009. "Characterization and photocatalytic property of Pd/TiO2 with the oxidation of gaseous benzene" *J Hazard Mater, 168*2-3, 1632-1635. doi:10.1016/j.jhazmat.2009.02.158

Zhu, X., Han, S., Feng, W., Kong, Q., Dong, Z., Wang, C., Lei, J.andYi, Q. 2018. "The effect of heat treatment on the anatase-rutile phase transformation and photocatalytic activity of Sn-doped TiO2 nanomaterials" *RSC Adv, 8*26, 14249-14257. doi:10.1039/c8ra00766g